Department of Environment, Land, and Infrastructure Engineering

Numerical Simulation on CO_2 Dissolution into Aquifers

Supervisores:

Prof. Carl Fredrik Berg (NTNU)

Prof. Dario Viberti (Polytechnic University of Turin)

Candidate:

Nima Hossein Zadeh

Thesis to obtain the Master of Science Degree in Geoenergy Engineering

July 2025

Abstract

As the world remains heavily reliant on fossil fuels as its primary energy source, a deepening concern has emerged regarding the release of human-generated carbon dioxide into the atmosphere. These emissions contribute significantly to the ongoing challenge of global warming.

An extensively recognized approach to address the challenge of carbon dioxide emissions is the capture and underground storage of carbon within geological formations. This method entails the extraction of carbon dioxide from various sources and its secure sequestration underground, thereby preventing its release into the atmosphere. Carbon capture and storage (CCS) offers the potential to continue utilizing fossil fuels while concurrently reducing CO_2 emissions by a substantial margin, up to 20%. The adoption of CCS may indeed emerge as a pivotal instrument in the pursuit of the global objective to restrict temperature increases to 2 °C.

Upon the injection of CO_2 into subsurface aquifers, various trapping mechanisms play a crucial role in preventing CO_2 leakage to the surface, ensuring secure sequestration. Among these mechanisms, dissolution trapping falls within the chemical trapping category, driven by the density difference between CO_2 and the brine in the formation. Molecular diffusion and convective mixing are the primary mechanisms that influence the dissolution rate. The timing of the start of dissolution and the point at which CO_2 achieves its maximal dissolution level in brine is critical, as free CO_2 can leak into the atmosphere through both caprock and wellbores during this important period.

This research explores the dissolution of CO_2 in a real system at laboratory scale and highlights the existing challenges, restrictions and some potential solutions to the challenges.

Acknowledgments

I would like to express my deep gratitude to my supervisor, Prof. Carl Fredrik Berg at NTNU for his guidance, support, and mentorship during the duration of this thesis. Furthermore, I am immensely grateful to my co-supervisor Prof. Dario Viberti at Politecnico di Torino for giving me a deep understanding in this topic which was the initiative for me to step ahead in this subject.

I am profoundly thankful to my family and friends for their unwavering love and support. Their guidance has played a crucial role in shaping the individual I have become.

My interest in the topic of simulation of CO_2 storage began when I took the course on underground fluid storage, where Prof. Viberti taught us about PVT variations when injecting a new fluid underground along with perfoeming simulations. Completing this thesis has been an enriching experience, filled with learning and growth. I hope that this work will contribute to the advancement of knowledge in CCS and inspire future research.

Nima Hossein Zadeh
Turin, Italy
July 2024

Table of Contents

List of Figures

1. Introduction

1.1 Global Warming

Global warming has been one of the most significant concerns of many countries in the world and it has become a problematic issue for the environment. It is the reason for climate change; thus, it affects natural ecosystems and weather conditions which then influence human life. One of the major basic reasons for it is the temperature rise which is due to the trapping of the solar radiation by some gases that is the greenhouse gas effect. These gases absorb the infrared radiation which is then converted into heat and leads to the temperature rise in the atmosphere. Different gases play a role in this cycle, among which CO_2 is considered the most significant. It not only has a huge contribution to absorption, but it also is increasing because of human activities such as the combustion of fossil fuels. Figure 1 shows the increasing trend of CO_2 in the past decades.

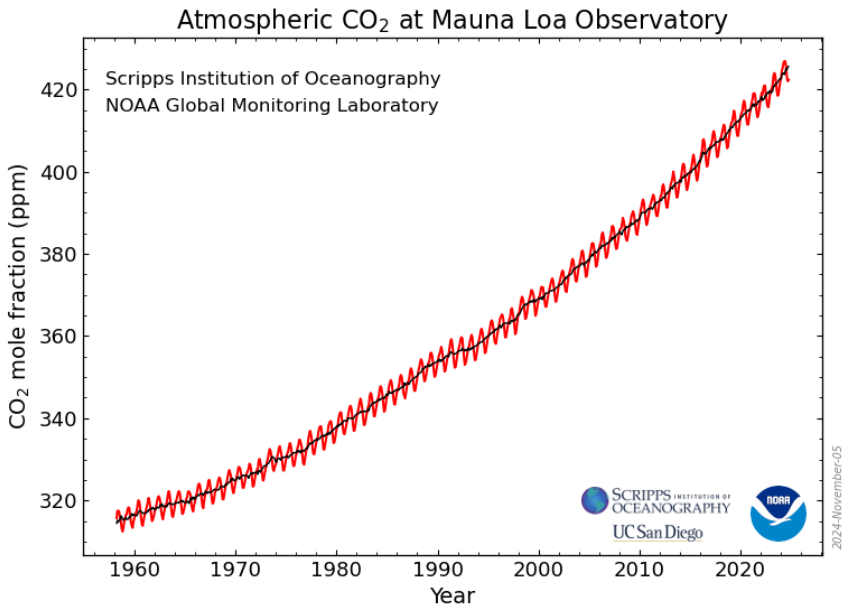

Figure 1- CO_2 mole fraction in the atmosphere in the past 60 years

According to the National Oceanic and Atmospheric Administration (NOAA) [1], the current amount of CO_2 is 422.38 ppm in October 2024. There are three options to mitigate increases in the atmospheric concentration of CO_2:

- Reducing carbon intensity by replacing fossil fuels with renewable or carbon-free energy sources, such as nuclear energy

- Improving energy efficiency
- Carbon capture and storage

Fossil fuels currently provide about 75% of the world's energy and will probably remain its major source until the end of this century, making the first suggestion difficult to realise [2]. The mitigation of the volume of CO_2 emissions into the atmosphere will therefore require a strategy involving carbon capture and storage.

1.2 Carbon Capture and Storage

CO_2 capture and storage (CCS) involves the capture, transport, injection and containment of CO_2 ingeological structures such as depleted oil and gas reservoirs, onshore and offshore saline aquifers and unmineable coalbeds located deep in the earth's crust. CCS is currently technically feasible, although large scale commercial CCS projects are yet to be developed. Many economies have pilot and demonstration projects to further the development of CCS technologies. Figure 2 shows how this process is done.

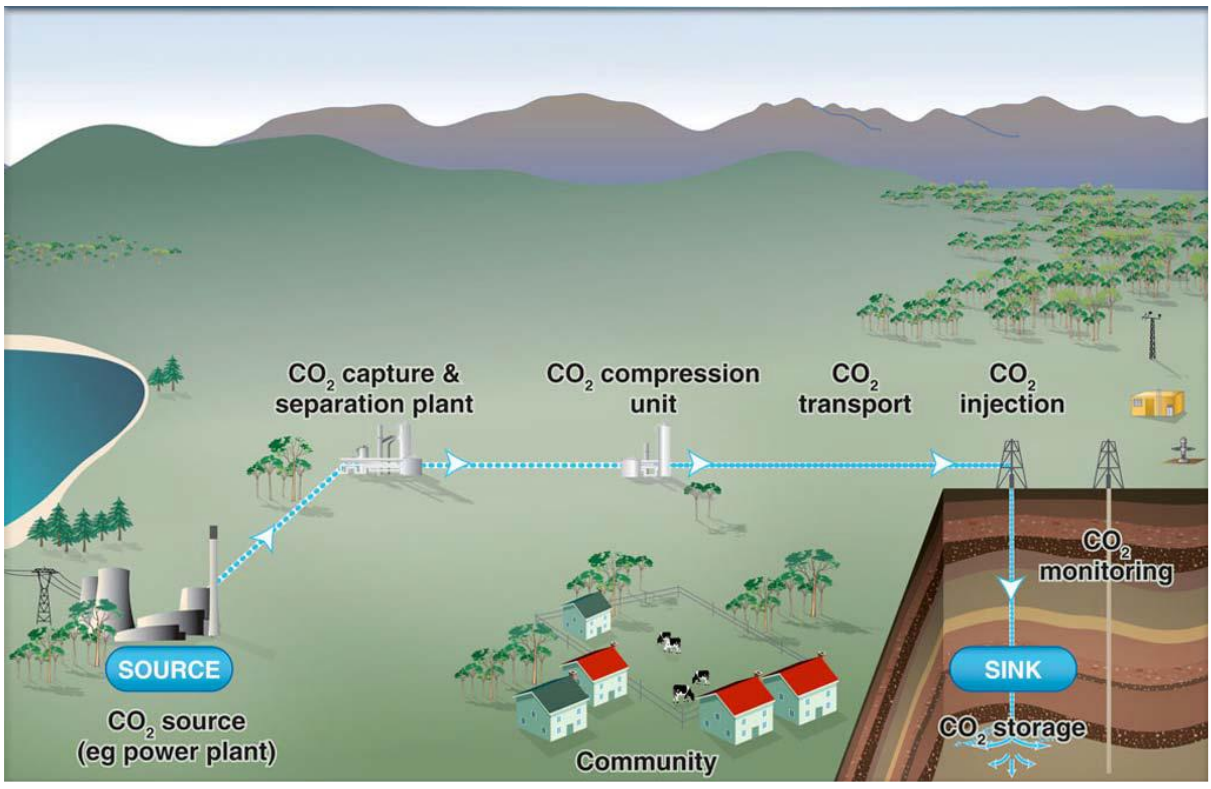

Figure 2- Overview of the components of carbon dioxide capture and storage

1.3 Geological Storage Sites

Within the domain of carbon capture and storage, the process of safely and permanently sequestering carbon dioxide in deep rock formations is commonly known as CO_2 geological storage. This crucial mechanism plays a critical role in preventing the emission of carbon dioxide into the Earth's atmosphere. Underground rock formations, specifically depleted oil or gas fields and deep saline aquifers, are primary targets for CO_2 sequestration owing to their porous characteristics. Although there are several porous rock formations, such as coal beds, shale units, volcanic rocks, and underground caves, that have been identified as potential solutions for CO_2 storage, their storage capacity is relatively less significant. Potential structures that have been considered in the literature are shown in Figure 3.

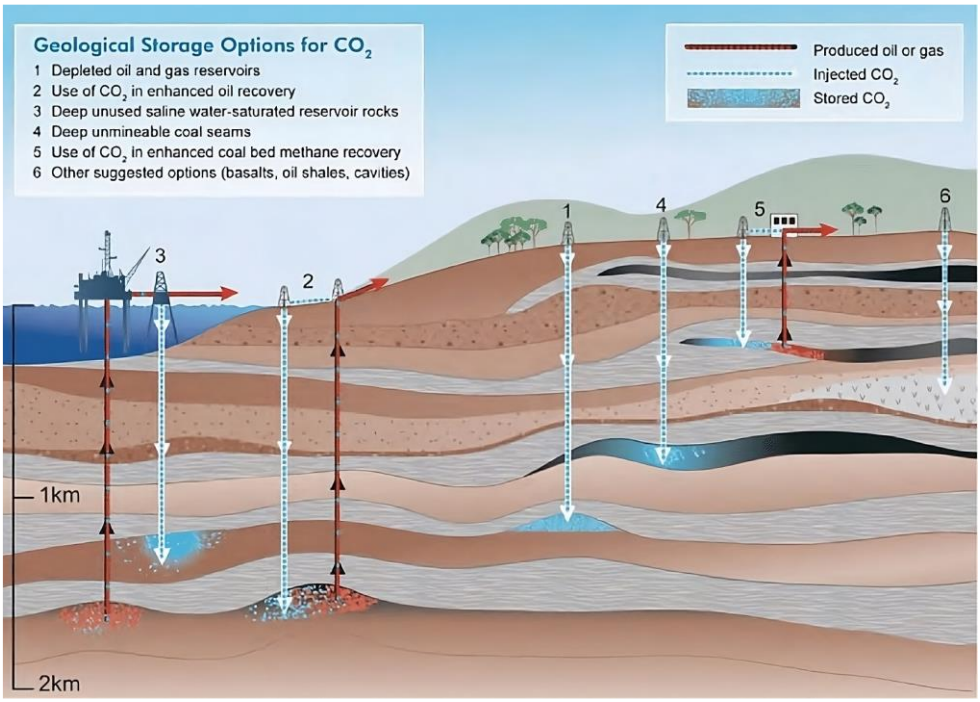

Figure 3- Possible underground storage methods of CO_2

Injecting CO_2 into depleted oil and gas reservoirs has the primary advantage of being economically beneficial to oil and gas production companies who seek to increase their recoverable reserves. CO_2 flooding is an effective tertiary recovery mechanism that uses established injection infrastructure and the vast technological experience of the oil industry to extend the profitability of many reservoir systems. While suitable formations are easily located, they have the distinct disadvantage of being inequitably distributed geographically [2]. Compared with oil and gas reservoirs, deep saline aquifers are widely distributed

throughout the globe, although often have poorly characterised geology. These systems could therefore be used for the disposal of anthropogenic CO_2 in locations where there are no suitable oil or gas reservoir alternatives.

1.3.1 Depleted Oil and Gas Reservoirs

A reservoir is depleted when it is no longer economically viable for hydrocarbon production, in other words, no longer possible to extract hydrocarbons. These reservoirs are prime candidates for CO_2 storage for several reasons. In fact, oil and gas have been originally accumulated and retained in these reservoirs for millions of years which demonstrates the containment and the integrity of the reservoir, however, it's important to ensure that extraction wells did not cause any damage that can cause a leakage pathway for CO_2. Additionally, these sites were already well characterized for the production phase and all physical and structural properties have been extensively studied, which can reduce data acquisition costs.

Most of these oil and gas reservoir rocks are made of sandstone, limestone, and dolomite, and they have enough porosity and permeability to support huge CO_2 volume injections. They also feature well-defined low permeability caprocks, such as shale, anhydrite, or tight carbonates, which restrict leaking into shallower strata. However, not all depleted reservoirs are equally suitable for CO_2 injection. Factors such as rock type, porosity, permeability, and fluid properties can influence the feasibility and effectiveness of CO_2 storage. Moreover, from the infrastructure side, existing wells and platforms can be potentially reused, which helps in reducing construction costs but also the condition of the wells should be assessed. From the storage capacity point of view, for hydrocarbon reservoirs with small water encroachment (small aquifer), the injected CO_2 will generally occupy the pore volume previously occupied by oil and/or natural gas. However, not all the pore space will be available for CO_2 because some residual water may be trapped in the pore space due to capillarity, viscous fingering effects [4]. For large aquifer support reservoirs, where pressure is maintained by water influx, in addition to the capacity reduction caused by capillarity and other effects, a significant fraction of the pore space will be invaded by water, decreasing the pore space available for CO_2 storage, considering that repressuring the reservoir is limited to preserve reservoir integrity.

1.3.2 Saline Aquifers

Saline aquifers are widely recognized as the most likely options for the geological storage of carbon dioxide. Due to the elevated salinity of the water contained within these subsurface rock formations, it is unsuited for human consumption [5]. In relation to the positioning of saline aquifers, three distinct categories can be distinguished: those that are situated beneath or above hydrocarbon reservoirs, those that are saline formations within the same geological structure as reservoirs, and those that are situated at a considerable distance from reservoirs [6]. One notable advantage of saline aquifers is their remarkable capacity for storing CO_2, which is estimated to be adequate for the containment of 10,000 gigatons. This value represents the emissions emitted by substantial stationary sources for more than a century [7]. Saline aquifers demonstrate a more extensive geographical reach and greater expanse in comparison to other alternatives for storing CO_2. As a result, they are inclined to be located in immediate proximity to sources of CO_2 emissions, which may result in decreased costs associated with the transportation of CO_2 [8]. On the contrary, the sequestration of CO_2 in saline aquifers poses specific difficulties attributable to infrastructure expenses and unpredictability. The assessment of saline aquifers frequently entails internal uncertainties, which complicates the process of forecasting the behavior of CO_2 after injection. Furthermore, the financial impact of injecting CO_2 into saline aquifers can be significant, particularly in cases where the aquifer is located far from pre-existing infrastructure. The potential consequences of pressure accumulation and CO_2 plume migration within the formation include formation fracturing, fault reactivation, and leakage. In regard to the sequestration of CO_2 in saline aquifers, these factors represent enormous challenges that demand meticulous evaluation [9].

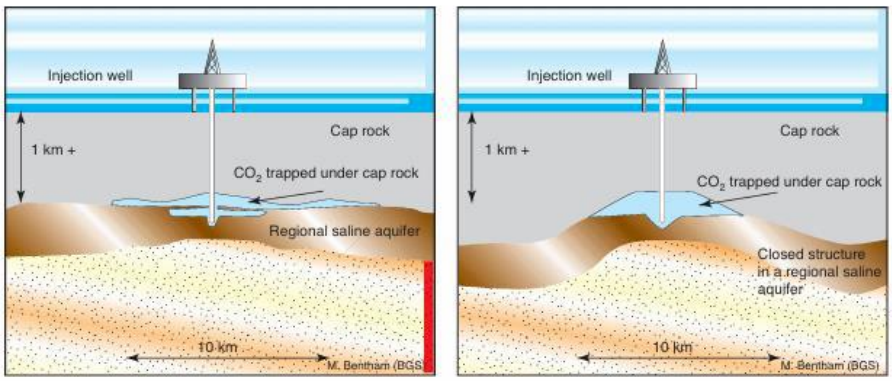

Figure 4- Different types of saline aquifers

1.4 Trapping Mechanisms

Carbon dioxide is injected into the subsurface and stored in the interconnected pore system. After injection, CO_2 starts moving in the system due to pressure differences or gravitational forces. The injected CO_2 will be trapped due to different mechanisms, which could be physical or chemical. Physical and chemical trapping mechanisms occur simultaneously but in different time scales. The concept of physical trapping involves the retention of injected CO_2's original physical properties upon its entry into an aquifer or reservoir, without undergoing any chemical conversions. The transport and distribution of CO_2 within the geological formation are restricted by low-permeable barriers [10]. On the other hand, chemical trapping arises via a series of geochemical reactions involving the injected CO_2, the brine present in the formation, and the adjacent rock. Throughout this process, CO_2 undergoes changes in both its physical and chemical properties, resulting in its absence in either a mobile or immobile state. This interaction effectively eliminates the existence of CO_2 as a separate phase, thereby substantially increasing the capacity for storage, which is especially advantageous for a long period of time [10]. It is worth mentioning that the phenomenon of physical trapping takes place just after the injection, but chemical trapping is a process that normally commences after a long time [11]. Figure 5 shows the proportionality of each trapping mechanism over time. The efficacy of the storage procedure relies on the collaborative operation of multiple trapping mechanisms to ensure a safe and effective long-term storage [5].

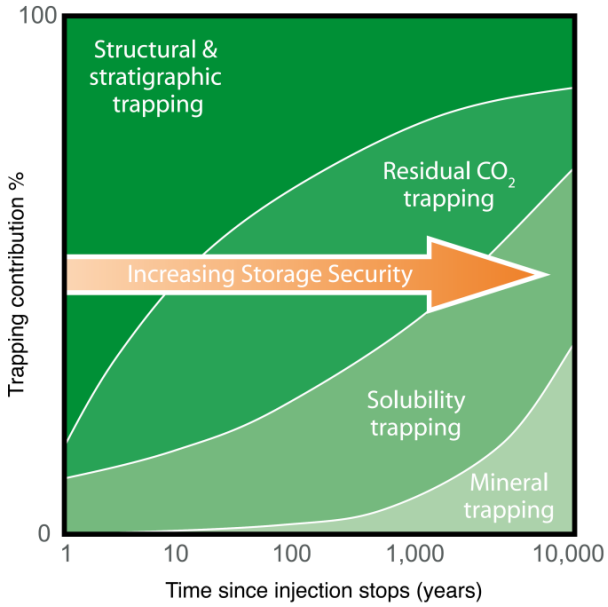

Figure 5- CO_2 trapping mechanism over time [12]

1.4.1 Structural and Stratigraphic Trapping

On a short time scale, structural or stratigraphic trapping is the principal trapping mechanism, representing a primary factor for screening candidate storage reservoirs. It involves a physical trap like a low permeability caprock, that inhibits the upward movement of mobile CO_2 toward drinking water aquifers and eventually back into the atmosphere. Suitable sealing formation characteristics would be considerable thickness and lateral continuity, geochemical and geomechanical stability, and absence of continuous and conductive faults. Even though structural trapping may keep the mobile fraction of the injected CO_2 underground, the free phase will still represent a leakage risk due to preferential flow pathways such as poorly sealed abandoned wells or fractures. A further process that has been proposed as a CO_2 trapping mechanism is hydrodynamic trapping [13], which involves the displacement of mobile CO_2 by the regional groundwater flow. The best storage scenario for this category of trapping would be represented by a low-dipping aquifer with a considerable flow gradient that will ensure a downdip in CO_2 movement toward regions of low potential, avoiding the need of stratigraphic barriers.

1.4.2 Residual Trapping

During the injection period of a typical storage scenario, the pressure of the CO_2 pumped into the reservoir is increased until the resident brine is displaced from the pore space, invading first the larger voids and gradually increasing the saturation of the plume. Once the injection ceases and the CO_2 pressure at the well suddenly drops, a redistribution of the fluids throughout the reservoir follows, producing a flow reversal in the saturation history and leading to an imbibition process. After the surrounding brine has displaced the mobile fraction of the plume from the pore space, isolated CO_2 droplets will be disconnected from the continuous phase, leading to its effective immobilization. The trapped fraction of CO_2 after the imbibition process is defined as residual saturation and is a function of the maximum CO_2 saturation, or initial saturation, reached at the time of flow reversal [14]. This residual trapping mechanism, also referred to as capillary trapping or relative permeability hysteresis trapping [15], is known to affect the flow of multiple fluid phases through porous media and it has been broadly studied in several areas of research. In contrast, the goal of CCS is to maximize the storage capacity of deep geological formations by increasing CO_2 immobilization through several trapping mechanisms, including capillary trapping. Therefore, estimation of

the residually trapped volume and saturation of CO_2 is fundamental for the assessment of trapping capacity of a potential reservoir.

1.4.3 Dissolution Trapping

Solubility trapping is a process that refers to the dissolution and hydration of CO_2 in the brine ($CO_2 + H_2O \leftrightarrow H_2CO_3$) to form carbonic acid in geological storage. CO_2 solubility in water increases with increasing pressure and decreases with increasing temperature and water salinity. As stated earlier, when CO_2 is injected into an underground reservoir, it experiences buoyancy due to the density contrast with the surrounding fluids. As a result, the CO_2 rises until it reaches an impermeable layer such as a cap rock. The CO_2 collects behind the cap rock, generating a plume that expands horizontally beneath the impermeable layer. Following this, CO_2 undergoes dissolution into the adjacent brine by mass transfer until a state of equilibrium is attained [16]. The process of molecular diffusion occurring at the interface between CO_2 and water in the reservoir facilitates the dissolution of CO_2 into the brine present in the formation. This process exhibits a very slow progression due to the significantly low molecular diffusion coefficient. As a result, it requires an extensive period, spanning thousands of years, for the complete dissolution of CO_2 in water to occur [17]. This greater density causes brine to move downward due to gravity, which speeds up the diffusion process and ultimately leads to a higher concentration of dissolved CO_2 in water [16].

1.4.4 Mineral Trapping

When CO_2 dissolves in brine it forms a weak carbonic acid. Carbonic acid, when combined with water, undergoes a chemical reaction with minerals present in the formation, leading to the production of solid mineral deposits referred to as carbonates. The rate at which this process occurs may be influenced by the concentration of acid [6]. The following reactions happen in this process:

$$H_2CO_3 \leftrightarrow H^+ + HCO^{-3}$$

$$HCO^{-3} \leftrightarrow H^+ + CO2^{-3}$$

They occur for pH values higher than 6. It is a preliminary step to mineralization, which will take place if Ca, Fe and Mg cations are available.

One notable attribute of mineral trapping is its inherent irreversibility, making it a highly permanent method of storage, frequently taking place after or simultaneously with solubility trapping. The effectiveness of this procedure is dependent upon various crucial elements,

such as the reservoir permeability and porosity, alongside the injection pressure of CO_2 [18]. Figure 6 shows how the sequence of solution trapping and mineral trapping occurs.

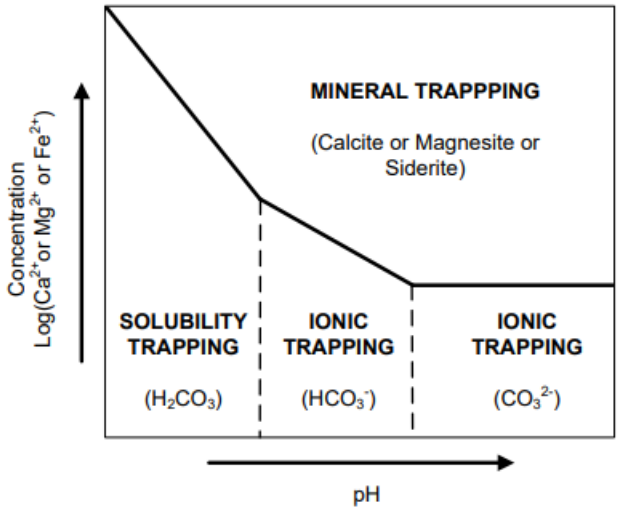

Figure 6- Geochemical trapping mechanisms for different pH and mineral concentrations

2. Theory

The dissolution trapping mechanism, as mentioned in the previous section, is a safe way of CO2 storage with almost no risk of leakage. This process is a result of different steps that occur in the molecular size. This section provides a detailed discussion of the steps involved to better understand the physics of the dissolution mechanism.

2.1 Diffusion

The process of gradual motion of concentration within a body, without net movement of matter as in the case of bulk flow, due to a concentration gradient is called diffusion. Bulk flow- the movement of a whole-body that occurs due to a pressure gradient. Diffusion results in a gradual mixing of material. It is characterized by the net flux of molecules from a region of higher concentration to one of lower concentration.

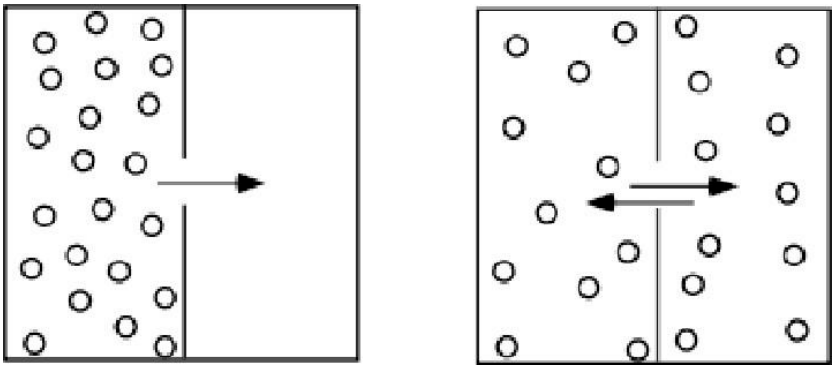

Figure 7- Diffusion as a consequence of existing special differences in concentration

2.1.1 Fick's law

Adolf Fick laid the foundation for understanding this fundamental process with his initial mathematical description in 1855. His groundbreaking work led to the formulation of two essential principles: the first law, governing steady-state, and the second law, which addresses transient diffusion [19].

In the context of steady-state diffusion, Fick's first law can be described as the diffusive flux which is directly proportional to the existing concentration gradient between areas with varying concentrations. Fick's First Law describes the flux of a species due to diffusion. It is expressed as [20]:

$$J = -D \frac{\partial C}{\partial x}$$

where J is the diffusion flux which is the amount of substance per unit area per unit time (kg/m^2.s), D is the diffusion coefficient (m^2/s), a property of the diffusing species and medium, and $\partial C/\partial x$ is the concentration gradient (kg/m^4).

This law assumes diffusion occurs in a steady state, where the concentration gradient does not change over time.

Fick's Second Law accounts for non-steady-state diffusion, where the concentration gradient varies with time. It is derived from the conservation of mass and the first law [20]:

$$\frac{\partial C}{\partial t} = -D\,\frac{\partial^2 C}{\partial x^2}$$

Where $\partial C/\partial t$ is rate of change of concentration with time (kg/m^3.s), and $\partial^2 C/\partial x^2$ is the second derivative of concentration with respect to position x, representing the curvature of the concentration profile.

2.1.2 Diffusion Coefficient

The diffusion coefficient is an unspecified parameter in Fick's laws, which characterizes the rate at which a substance moves from an area of higher concentration to an area of lower concentration as a result of the random movement of molecules. In other words, the term "Diffusion Coefficient" refers to the inherent ability of a material to disperse within a specific medium [21]. The importance of the diffusion coefficient is to provide information about the system. Since different substances possess different diffusion coefficients their definition will give an idea about the matter. The change in system properties will lead to an alteration of the diffusion coefficient. For instance, increasing the temperature of the system results in the enlargement of the diffusion coefficient. This is because molecules have a larger thermal movement.

2.1.3 Dissolution rate

The basic definition of molecular diffusion which also is stated earlier in this chapter, argues that molecules move in whatever medium they are localized, at a specified rate, and in a random manner. In addition to the concentration gradient, the mass of molecules, the environment that molecules are in, and the molecule's thermal energy, which is a function of temperature, all are parameters that highly affect the rate of the molecular diffusion. A brief explanation of each parameter will be provided below [22]:

• Concentration: As mentioned earlier, molecular diffusion is highly dependent on the molecule's displacement from a higher concentration area to a lower concentration area. In other words, the phenomena occur in the direction of the gradient in concentration of a particular molecule. A higher difference in concentration yields faster displacement, and a lower difference in concentration results in deceleration of molecule movement.

• Temperature: Particle motion is a consequence of the kinetic energy they possess. An elevation in temperature induces an augmentation in the kinetic energy of molecules, thereby facilitating the acceleration of particle motion. As a result, an escalation in the motion of particles would lead to rapid diffusion. On the contrary, a decrease in the kinetic energy of particles will result in a reduction in the velocity of the diffusion process.

• Mass of molecules: The movement of a particle depend on the mass of the particle. A slower movement will associate to a particle with higher weight, which in turn decreases the rate of diffusion process. On the other hand, molecules with smaller weights have the potential for faster diffusion because of their capability for rapid movement.

• Medium properties: Both viscosity and density play important roles in the diffusion process. A particle faces increased resistance and obstacles during diffusion when traversing a medium that is extremely dense or viscous; therefore, the rate of diffusion is reduced. In contrast, the diffusion rate increases when particles can move more quickly through a medium that is less dense or less viscous.

2.2 Convective mixing

Convective mixing is the process of combining two sets of solid particles so that they disperse into one another. In the process of CO_2 sequestration in saline aquifers, convective mixing plays an important role in the long-term trapping of CO_2 underground. The dissolution rate is determined by the rate at which undersaturated brine encounters CO_2, whether through diffusion or convection. Notably, convective mixing accelerates the dissolution rate by effectively spreading CO_2 across the aquifer [17]. As a result, knowing the role of convective mixing in CO_2 sequestration and the timescales involved becomes important. The duration of CO_2 dissolution into brine is a significant measure because it represents the time when the injected CO_2 is susceptible to leaking into the atmosphere through both caprock and wellbores [23].

2.2.1 Onset of Convection

Once CO_2 is injected into the saline aquifer and creates a plume behind stratigraphical and structural traps, supercritical CO_2 gradually diffuses into the surrounding brine, making the mass transport of CO_2 diffusion-controlled, as mentioned before. Subsequently, fingers begin to form and grow linearly. As the process continues, there is a rise in CO_2 dissolution flux. The fingers eventually merge, leading to the initiation of natural convection, which enhances both dissolution and mixing. Finally, the dissolution flux of CO_2 diminishes, marking the onset of the "convective shutdown" regime [24]. Convective dissolution is driven by the interaction of an unstable fluid density field and internal disturbances within the system [25]. The instability arises from the presence of a higher-density fluid positioned above a lower-density one. Specifically, in the context of dissolution trapping, this instability occurs because of CO_2 dissolving in brine and the. The critical time which gives the theoretical earliest onset of convective mixing is

$$t_{crit} = 48.7D\left(\frac{\varphi\mu}{k\Delta\rho g}\right)^2$$

Where D, φ, μ, Δρ, g, and k are diffusion coefficient, porosity, brine viscosity, maximal mass density increase for fully CO_2 saturated brine, acceleration of gravity, and absolute permeability respectively [26].

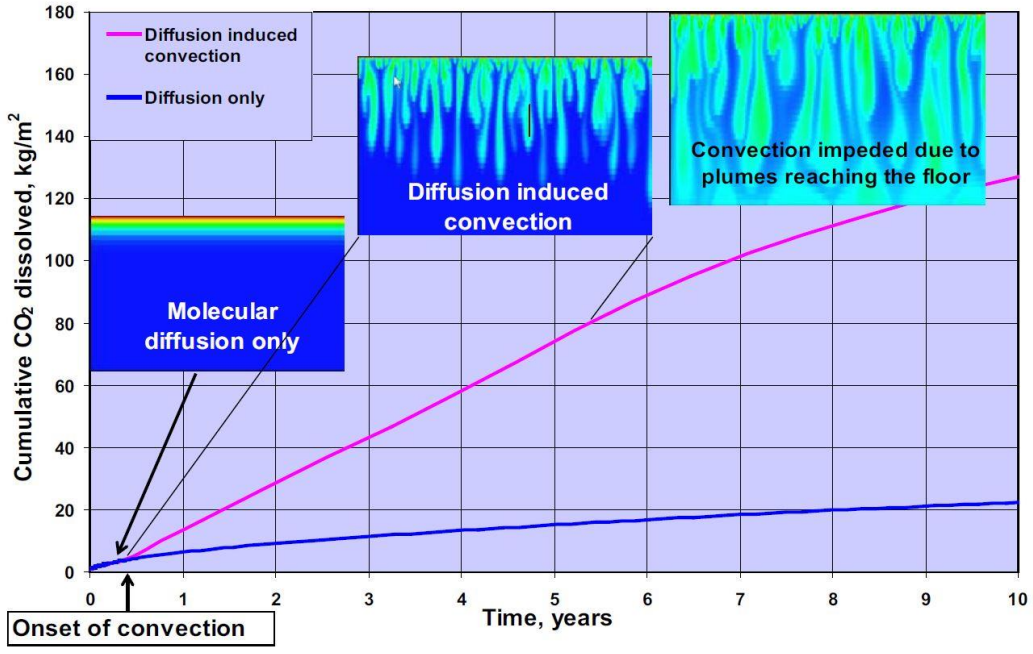

Figure 8- Cumulative CO_2 dissolved over time for diffusion-only and diffusion-induced convection

3. Experimental Setup

For better understanding of density-driven-convection mechanism in CO_2 storage into brine aquifers, this mechanism was investigated in a laboratory tank. The tank consists of a porous media made with silica bead pack; one injector well located in the middle of the top part with four connection points which is controlled by a pump to keep the pressure of the tank constant and one producer in the middle of the bottom part of the tank to drain water. The tank is 60 centimeters both in height and diameter. The silica bead pack fills the tank up to 13 millimeters from the top and tank is initially fully saturated with deionized water. The wells are opened to inject CO_2 from the top and drain water from the bottom until the 13 millimeters void space is saturated with CO_2. During this process, the pressure of the tank is constant and is 60 bar. After that, the producer is shut in and the injector continues injecting but with a lower rate to only keep the pressure of the tank constant at 60 bar. Table 1 shows the experiment setup and fluid properties.

Table 1- Properties of the tank, porous media, and the fluids

System Parameter	
Internal diameter	60 cm
Height of bead pack	58.7 cm
Headroom above bead pack	1.3 cm
Process pressure in experiment	60 bars
Process temperature in experiment	20.0 °C
Permeability of bead pack	20000 mD (approximately)
Porosity of bead pack	0.40
Water composition	De-ionized tap water
CO2 composition	Pure
Bead material	Silica beads, 70-100 µm grains

The Experiment shows that the onset of convection happened sometimes between 50 to 100 hours, which is confirmed by the numerical simulation results explained in the next section.

4. Numerical Model

In parallel to the laboratory experiment, a numerical simulation has been performed to investigate this trapping mechanism in detail and compare the onset of convection with the one measured in the laboratory. Eclipse 100 [27], a black oil simulator, is used to perform the simulations and ResInsight [28] is used as 3D visualizer and post processing reservoir simulations.

The model is a 3D symmetric cylindrical reservoir with the same size as the laboratory tank (60cm in diameter and height). The two fluids introduced to the model are oil and gas. The PVT properties of oil is set to be the PVT of water and those of gas is the PVT properties of CO_2. To simulate the diffusion, process the keyword "DIFFUSE" is used in the datafile and the corresponding diffusion coefficient of CO_2 in water is used from the literature [29].

The actual porous media properties are used (as shown in table 1) in the simulations with 0.5 percent perturbation to both porosity and permeability. To represent the experiment condition, the porosity and permeability of the top part of the tank is set to be high enough such that it is a void space. Two wells are defined, one injector with four connections and one producer, at the top and bottom part of the tank respectively.

The tank is initially saturated fully with water at 60 bars. There is no free or dissolved gas at initial condition. Both wells are opened from the beginning of the simulation to inject CO2 from the top and drain water from the bottom with a constant rate at 60 bars up to the point that the void space is fully saturated with the gas. Then, the producer will be shut in and the injector continues to inject with a very low rate only to prevent pressure decline due to the dissolution of the gas into water and keep the pressure of the tank constant at 60 bar. Figure 9 shows a schematic of the beginning of the simulation. The injection is done at the center where the well is located, and the four other points connected to the main injector. As can be seen in the figure, the gas rapidly moves laterally to fill the void space. The capillary pressure at the interface between the void space and the porous media prevents the downward movement of CO_2 at the filling step and this also contributes to the lateral movement of the gas indirectly.

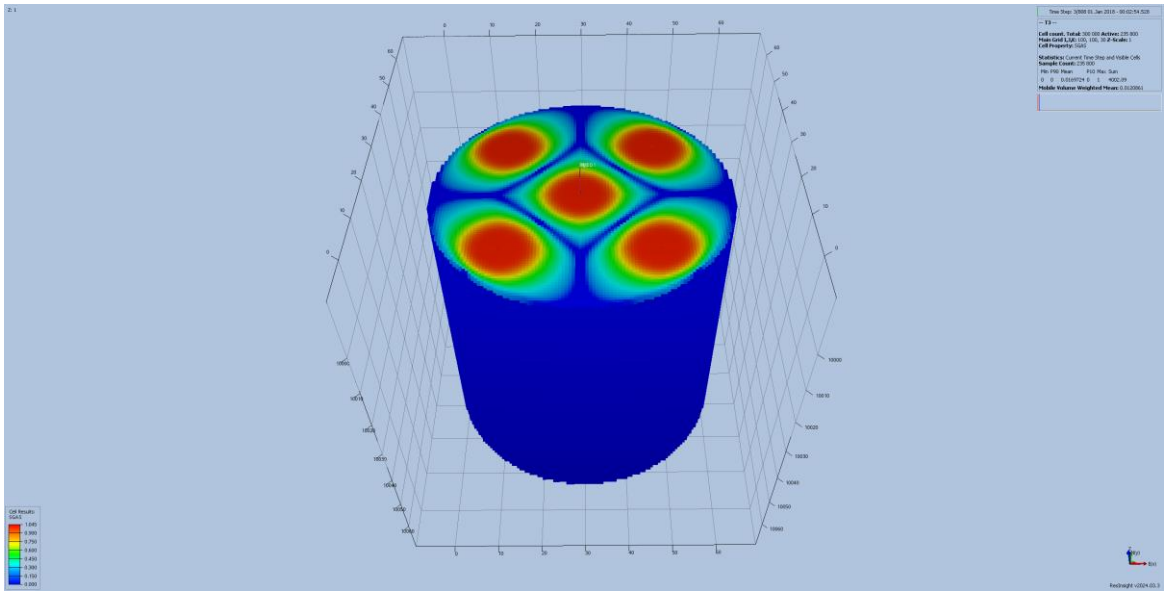

Figure 9- Distribution of CO_2 saturation as a free gas at the very beginning of the simulation

Figure 10 shows a side view of the tank after the void space has been saturated with CO_2. By this time, there is a gas cap at the top part and a porous media filled with water as an aquifer below the gas cap. This is an ideal condition where we can monitor dissolution of CO_2 into the water over time.

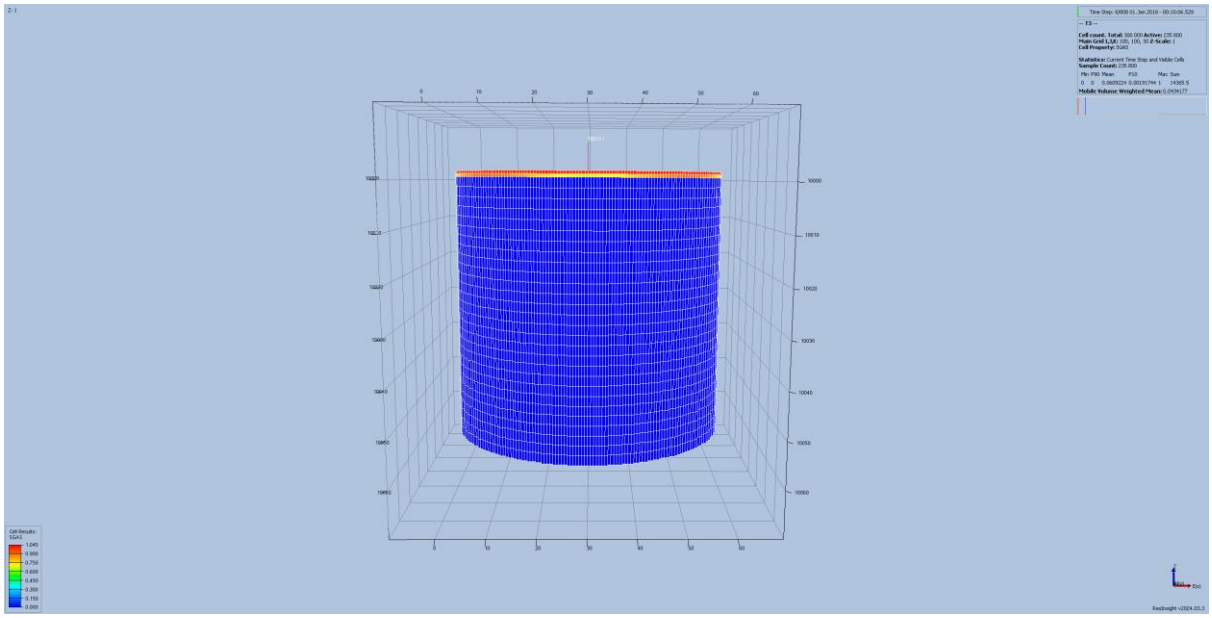

Figure 10- Side view of the tank after injection of CO_2 to fully saturate the void space

4.1 Relative Permeability and Capillary Pressure

As discussed previously, capillary pressure has significant effect in preventing the gas from interning the porous media and early time of injection and it helps the gas to fill the void space fully and rapidly. The relative permeability on the other hand, has minor effect in the process since the phases are separate at the beginning. After the dissolution of the CO_2, still we have single phase fluids in the tank, so the relative permeability will not have a huge impact on the whole process. Thus, the relative permeability values are set to be linear in the void space but to account for any minor impact of it, the Brooks-Corey parameterization is used to calculate relative permeabilities and capillary pressures in the porous media [30]:

$$K_{rw} = (S_w^*)^4 \ , \qquad K_{rn} = 0.4\,[1 - (\hat{S}_w)^2](1 - \hat{S}_w)^2$$

$$S_w^* = (S_w - S_{wi})/(1 - S_{wi})$$

$$\hat{S}_w = (S_w - S_{wi})/(1 - S_{wi} - S_{nc})$$

$$P_c = P_{c,e} \times \left(\frac{S_w - S_{wi}}{1 - S_{wi}}\right)^{-0.5}$$

where the irreducible water saturation (S_{wi}) is 0.2, the critical CO_2 saturation (S_{nc}) is zero, and the capillary entry pressure ($P_{c,e}$) is 0.2 bar. The subscripts w and n denote the wetting (water) and nonwetting (CO_2) phases, respectively. The relative-permeability and capillary-pressure curves are also plotted in figure 11.

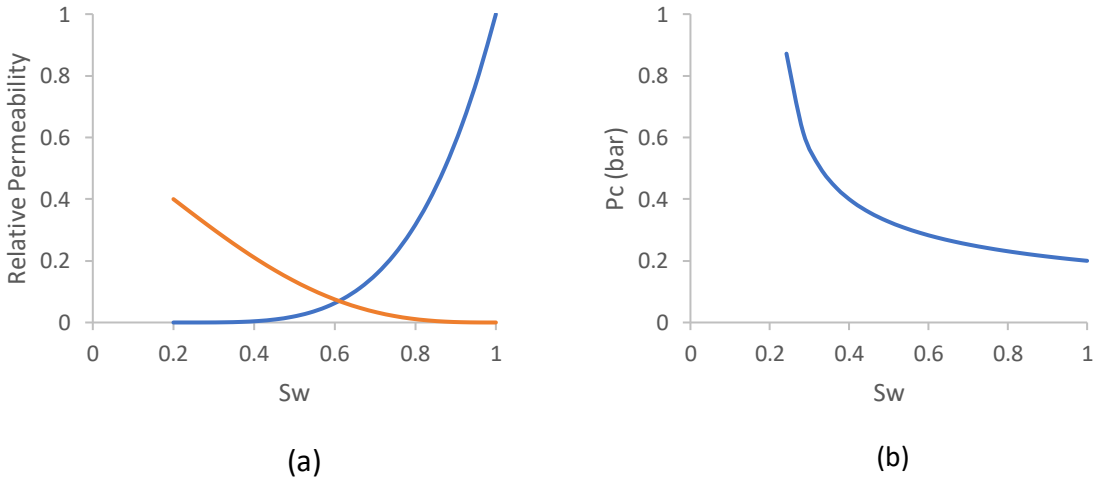

Figure 11- (a) Relative-permeability curves; (b) Capillary-pressure curve.

To define linear relative permeability in the void space and implement the Brooks-Corey method, two saturation regions are defined using “SATNUM” keyword in Eclipse datafile in the model, one for the void space which accounts for 20000 cells and one in the porous media which accounts for the remaining 280000 cells.

4.2 Dissolved Gas and dissolution rate

Calculating the amount of dissolved gas is a good indicator of the dissolution mechanism and can give an idea of how much this mechanism can contribute to the storage of CO_2. Also, by knowing the amount of dissolved gas, or the rate of dissolution which can be derived from it, it would be possible to estimate how much CO_2 can be further injected into the system, and how the pressure will vary due to dissolution and injection.

To calculate the amount of dissolved gas (R_s), a python code is written. By using some of the python library and a ‘’ecl2df’’ ,a library designed to facilitate the extraction of data from Eclipse reservoir simulation file which simplifies reading and processing Eclipse's binary output files (like .DATA or .UNRST files) and converts the data into pandas DataFrames for easier analysis and visualization, it is possible to calculate the average Rs for each timestep and plot them over time.

The procedure begins by loading the Eclipse reservoir simulation data and extracting grid-based properties for all timesteps. The relevant data columns for dissolved gas-oil ratio (R_s) and gas saturation (S_{gas}) are identified. Oil saturation (S_{oil}) is calculated for each grid cell and timestep using:

$$S_{oil} = 1 - S_{gas}$$

The data is then refined to include R_s, S_{oil}, and pore volume (PORV) for all timesteps. For each timestep, the weighted R_s is computed for every grid cell using:

$$R_s(weighted) = R_s \times S_{oil} \times PORV$$

These weighted values are summed across all grid cells, and the pore-volume-averaged Rs for each timestep is calculated as:

$$Pore - volume - averaged\ R_s = \frac{\sum(R_s \times S_{oil} \times PORV)}{\sum(S_{oil} \times PORV)}$$

This calculation aggregates the contribution of each grid cell based on oil (used instead of water) pore volume.

The python script written to obtain Rs is the following:

```
import ecl2df

import pandas as pd

import numpy as np

import matplotlib.pyplot as plt

from ecl2df import grid


def process_eclfiles(file_path, grid_range):

    # Load the Eclipse data file

    eclfiles = ecl2df.EclFiles(file_path)

    df = grid.df(eclfiles, rstdates='all')

    df = pd.DataFrame(df)


    # Filter rows for the specified grid range

    df_1 = df.iloc[grid_range]


    # Identify columns for Rs and Sgas

    Rs_col = [col for col in df_1.columns if col.startswith('RS@')]

    Sgas_col = [col for col in df_1.columns if col.startswith('SGAS@')]


    # Create a DataFrame with only the Rs and Sgas columns

    df = df_1[Rs_col + Sgas_col]


    # Calculate oil saturation (Soil) as 1 - Sgas for each timestep
```

```
    for Sgas_coll in Sgas_col:
        time_step = Sgas_coll.split('@')[1]
        df[f'SOIL@{time_step}'] = 1 - df[Sgas_coll]

 # Extract the Soil columns
    Soil_col = [col for col in df.columns if col.startswith('SOIL@')]
    df = df[Rs_col + Soil_col]
    df['PORV'] = df_1['PORV']

 # Calculate weighted Rs for each timestep
    for Time_step in Rs_col:
        Rs_val_col = f"RS_val{Time_step[-10:]}"
                            df[Rs_val_col]      =      df[Time_step]      *
df[Soil_col[Rs_col.index(Time_step)]] * df["PORV"]

    # Sum Rs weighted values for pore-volume averaging
    Rs_val_col = [col for col in df.columns if col.startswith("RS_val")]
                Rs_f        =        df[Rs_val_col].sum(axis=0)        /
(df[Soil_col[Rs_col.index(Time_step)]] * df["PORV"]).sum(axis=0)
    return Rs_f

def main_plot():
    Rs_f = process_eclfiles('R2.DATA', slice(None))
    t_steps = [str(step)[-10:] for step in sorted(set(Rs_f.index))]
    plt.figure(figsize=(12, 8))
    plt.plot(t_steps, Rs_f, linestyle='.', color='b')
```

```
    plt.xlabel("Time [Days]")
    plt.ylabel("RS [scc/scc]")
    plt.title("RS Vs. Time for R2.DATA")
    plt.xticks(rotation=90)
    plt.tight_layout()
    plt.savefig('Rs_R2_DATA.png')
    plt.show()
if __name__ == "__main__":
    main_plot()
```

The obtained figure is the following:

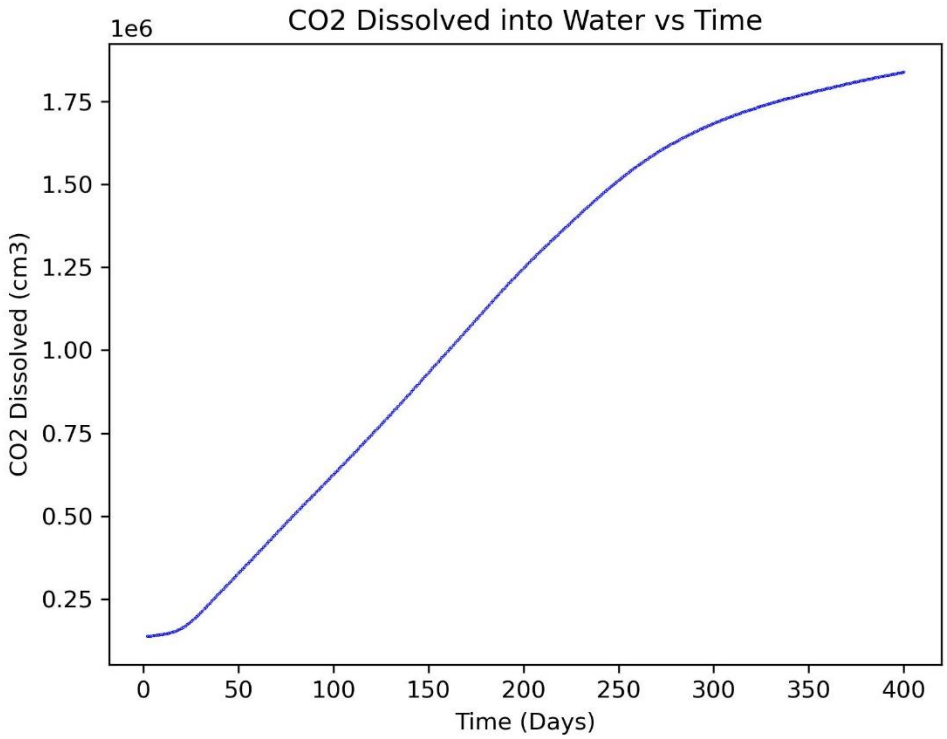

Figure 12- The amount of CO_2 dissolved in water (Rs) over time

To analyze the rate of dissolution of the CO_2, the time-series data of dissolved CO_2 volume were extracted and processed using Python. The dissolution rate was calculated by applying

a numerical differentiation via the gradient method which yields the derivative of Rs with respect to time (dRs/dt). The Python script written to obtain the dissolution rate is the following:

```
import pandas as pd

import numpy as np

import matplotlib.pyplot as plt


# Step 1: Load the data file

file_path = r'C:\Users\Nima\Desktop\thesis\final\uniform grid - base case\daily FGIPL plot data .xlsx'  # Your file path

data = pd.read_excel(file_path)

data.columns = ['Time', 'CO2_Dissolved']

x = data['Time'].values

y = data['CO2_Dissolved'].values


# Step 2: Calculate the numerical derivative (dissolution rate) for the entire dataset

dissolution_rate = np.gradient(y, x)


# Step 3: Plot the dissolution rate for the entire dataset

plt.figure(figsize=(10, 6))

plt.plot(x, dissolution_rate, label="Dissolution Rate", color="purple", linewidth=2)


plt.xlim(left=0)  # Set the x-axis to start at 0

plt.ylim(bottom=0)  # Set the y-axis to start at 0

plt.ylim(bottom=0, top=7000)
```

```
plt.xlabel("Time(days)")

plt.ylabel("Dissolution Rate (dRs/dt) (cm3/s)")

plt.title("Dissolution Rate  vs. Time ")

plt.axhline(0, color="black", linestyle="--", linewidth=0.8)

plt.legend()

plt.grid()

plt.tight_layout()

plt.show()
```

The obtained figure is the following:

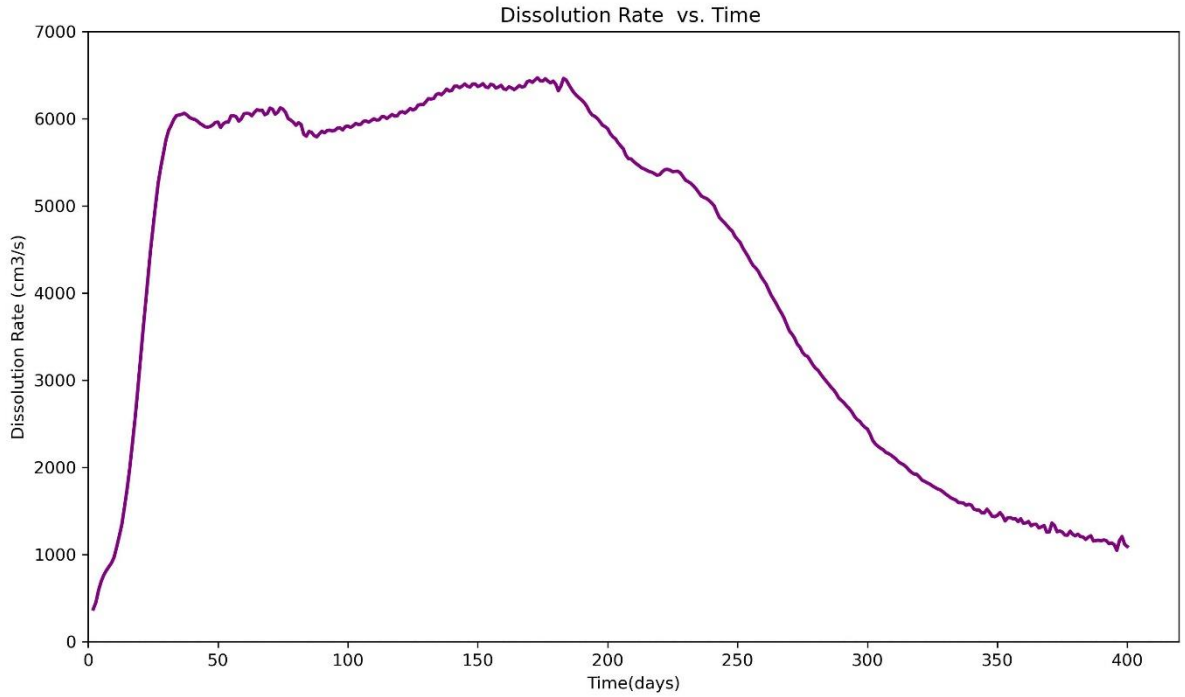

Figure 13- The rate of CO_2 dissolved in water over time

5. Results and Discussion

This section will discuss various dissolution regimes which are established during injection and post-injection, and they will be highlighted in the figures obtained from the simulations mentioned in the previous section. Three regimes can be captured while injecting CO_2 into the saline aquifers and they can be observed separately in the dissolved CO_2 curve in water. However, they will not disappear as the system move forward to and continue to occur at smaller scale. This means that these flow regimes always coexist in the system, but in each period, there is only one of them which is governing the flow regime of the fluids.

To capture these regimes a linear analysis of CO_2 dissolution behavior over time is performed by dividing the time-series data into three distinct regions and fitting a separate linear regression model to each segment. These fitted lines help to capture the initial diffusion-dominated phase, a transitional region which the convective mixing, and a late-time convection-enhanced phase. Extrapolations of the fitted lines are used to estimate their behavior beyond the defined regions, allowing the identification of a crossing point between the first and second, and the second and third segments. This intersection represents the estimated onset of a new flow regime, such as the shift from diffusion to convection. Figure 14 shows how different segments can be determined with the linear regression.

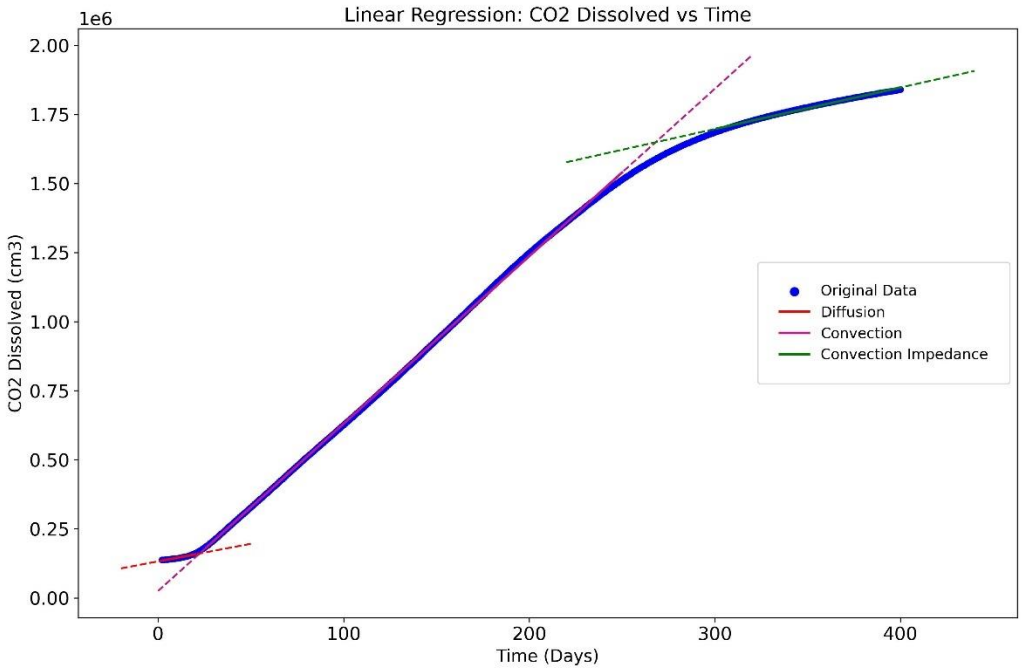

Figure 14- Linear regression of CO_2 dissolved versus time to identify distinct dissolution regimes

5.1 Diffusion

Molecular diffusion is the first regime which happens at the very early time of the injection. As the injected gas (CO_2) reaches the water surface depth, it starts to diffuse into the water. As mentioned previously, diffusion is a slow process that occurs without the presence of flow and only due to concentration gradient of the gas between the gas phase and the liquid phase. Therefore, at this stage the amount of dissolved gas and the rate of dissolution is relatively low.

As diffusion continues and more gas dissolves into the water which increase its density, it induces a gravity effect and eventually convection. In reality, diffusion induced convection happens as the system moves forward. However, an extraploation to Rs curve over time during diffusion indicates an approximation of the pure diffusion contribution to CO_2 dissolution. This means neglecting the effect of gravity, which is the main reason for convection, to asses the diffusion only.

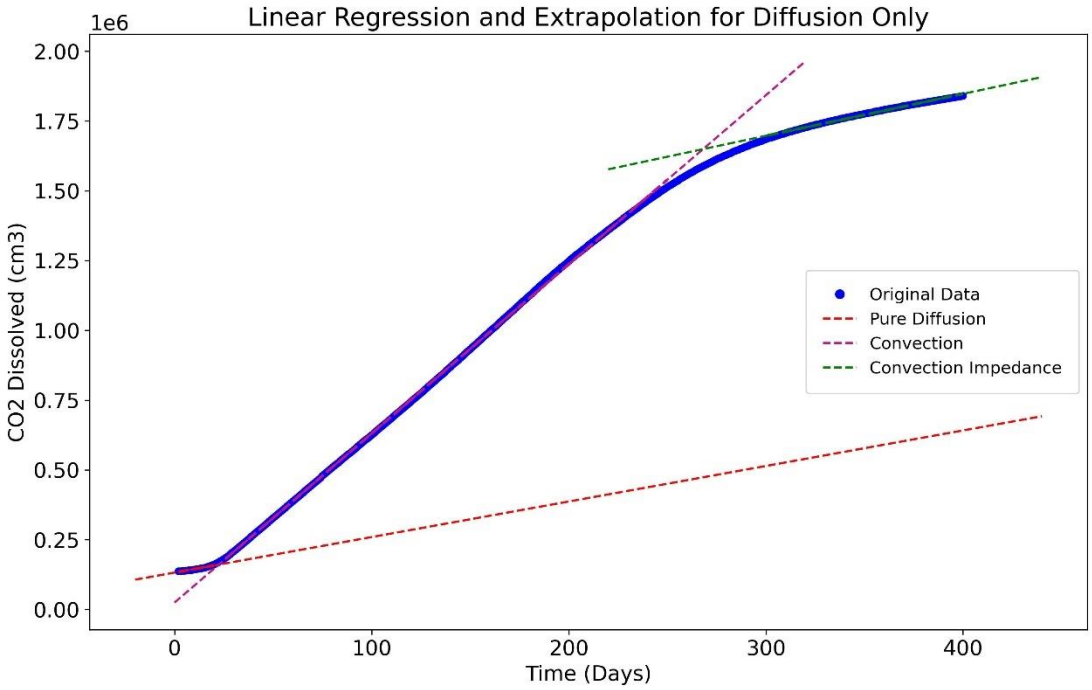

Figure 15- Linear regression and extrapolation to assess pure diffusion

5.2 Convection

Convection regime has the most significant effect in the dissolution of the gas into the water. During this period, a huge amount of gas dissolves in water and the rate of dissolution increases significantly, as depicted in figure 12 and 13, respectively.

5.2.1 Onset of Convection

The time when the convection begins is the onset of convection. This is when enough gas is dissolved into the water due to diffusion which induce a density contrast between the water with dissolved gas and pure water. Although convection happens gradually and there is transition time from diffusion to convection, it is important to estimate a time at which the system behavior is governed by the convection regime. This is a critical time which can influence any decisions on injection strategies.

To estimate the onset of convection for the model in this study, an extrapolation of the linear regression is performed for the diffusion and the convection zones. The intersection point is the approximation time for the onset of convection.

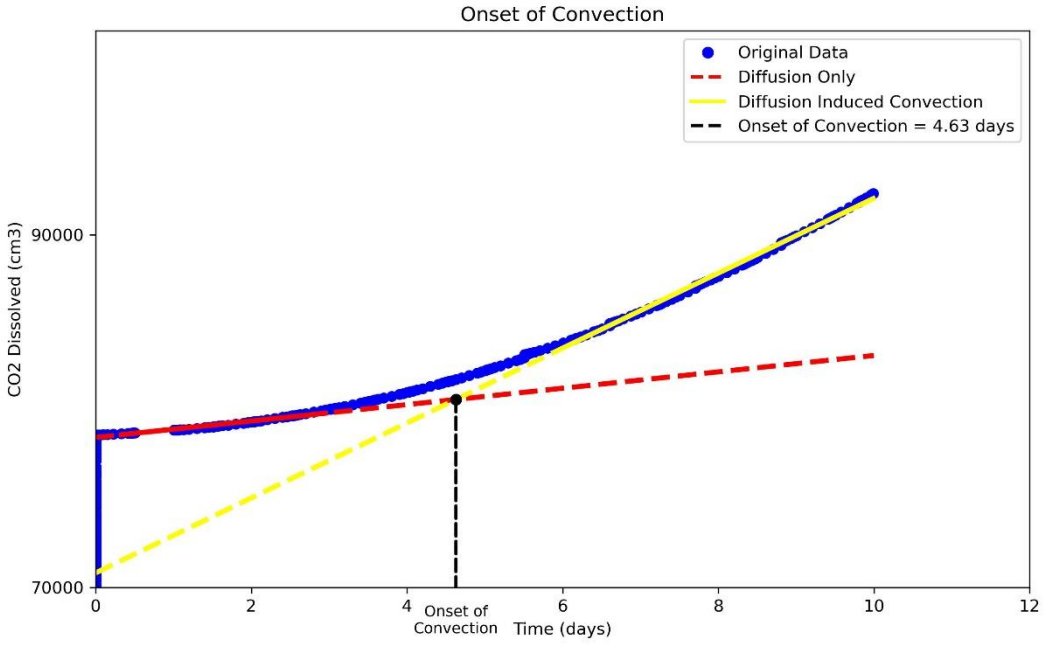

Figure 16- Estimating the onset of convection with linear regression and extrapolation

The onset of convection estimated is about 4 and a half days which is almost the same time as the one observed in the experiment (between 50 to 100 hours).

The snapshots below are captured at some times before, after and at the onset of convection, and they are approximately confirming that the convection cycles are starting at the estimated time. Figure 17 shows how CO_2 is dissolving into the water a few days prior to the convection onset and the dissolution distribution almost fully covers the top water levels.

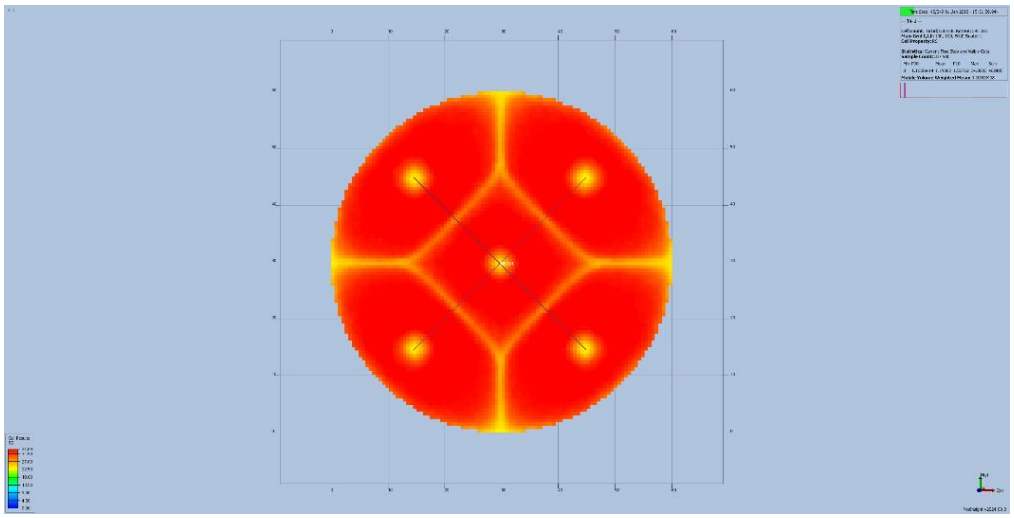

Figure 17- Top view of the model (solution gas water) 3 days before the onset of convection

As the system moves forward and the convection begins, it is visible that in some portions of the model, fresh water moved upward and replaced some of the water with dissolved CO_2 which means the convection has started to happen. This can be clearly observed in figure 18.

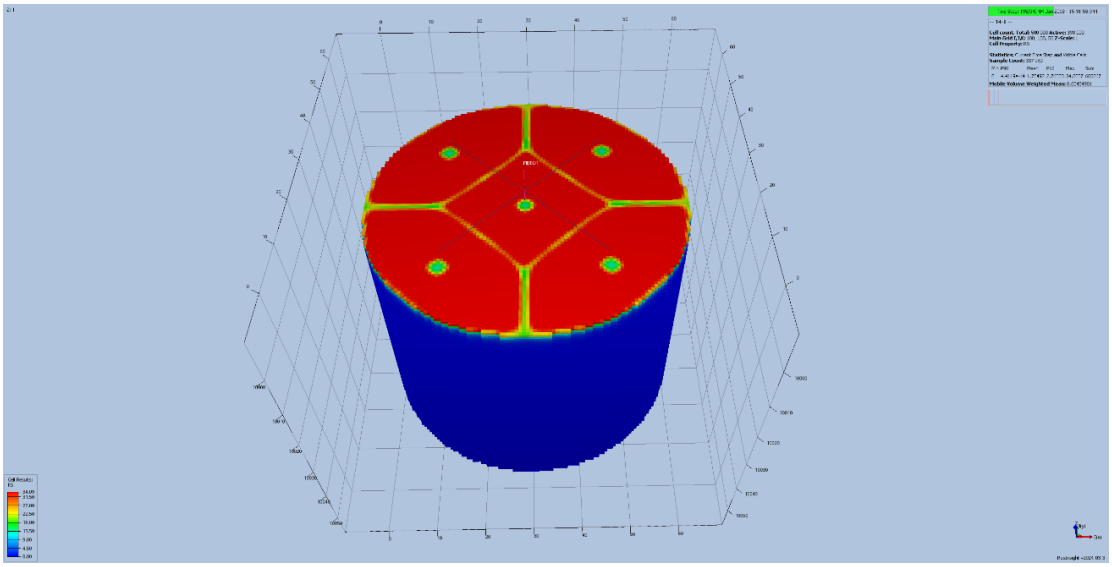

Figure 18- Dissolution distribution at the onset of convection

Figures 19 and 20 show the same timestep as figure 18, but the first two layers in the Z direction is filtered out to observe how the water with dissolved CO_2 is moving downward and the fresh water is replacing it in the above levels.

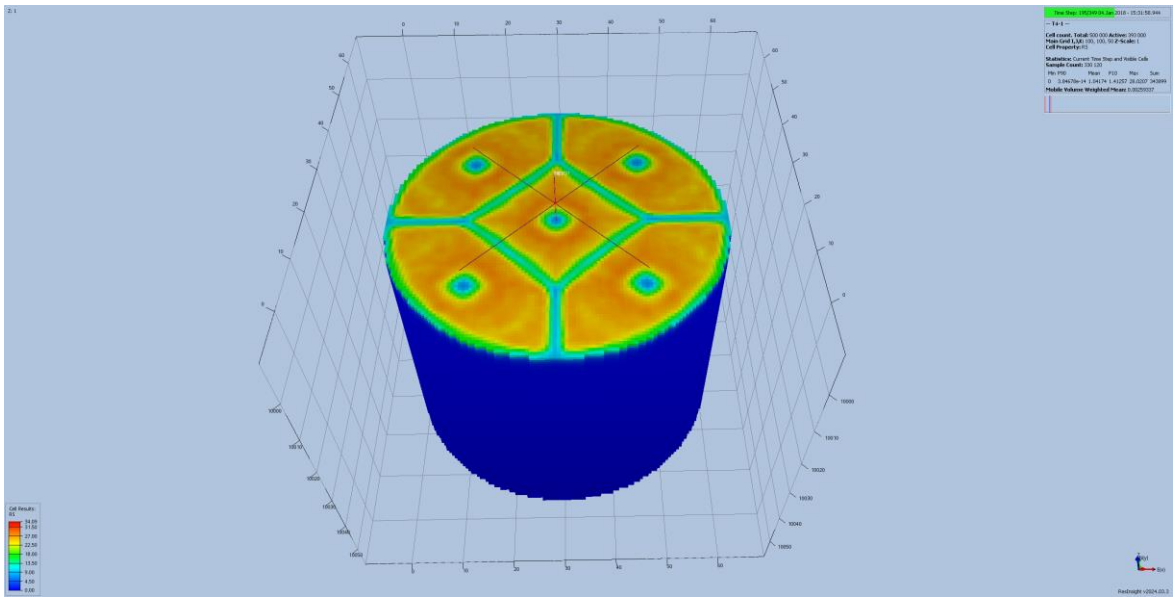

Figure 19- Dissolution distribution at the onset of convection; the first layer is filtered out.

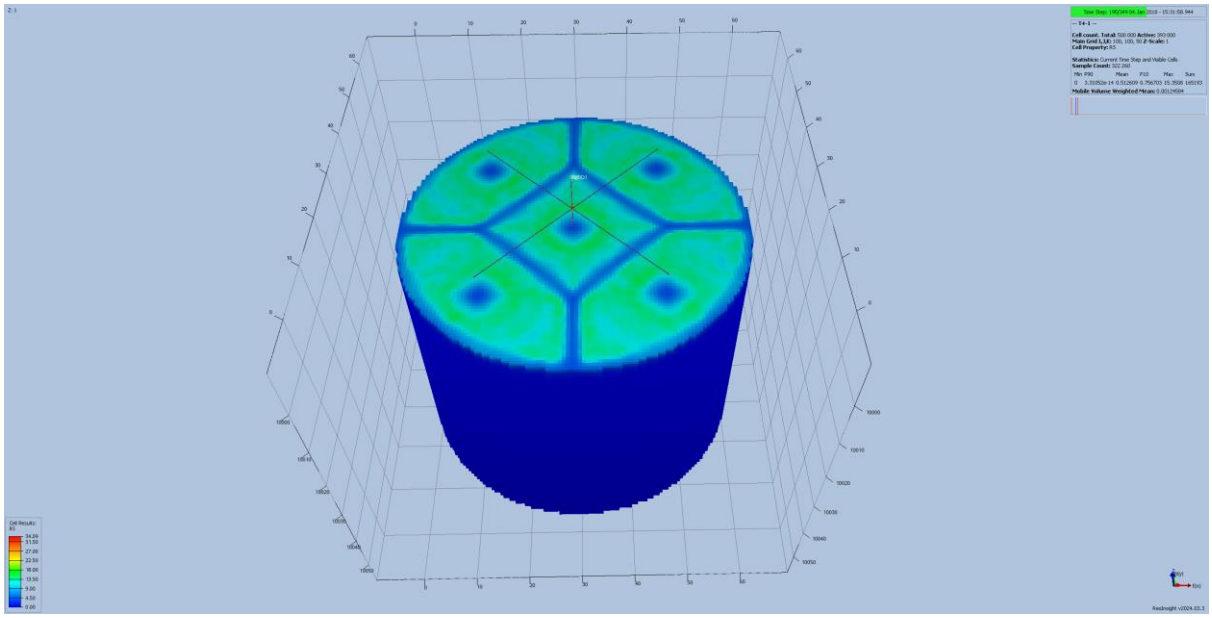

Figure 20- Dissolution distribution at the onset of convection; the first and second layers are filtered out.

5.2.2 Development of convection

As more gas is dissolved into the water, the water becomes heavier in terms of density. This happens in the region where gas is in contact with the water, while the water in the deeper depth is still pure, thus it is lighter than that of the upper part. Due to this density contrast and the gravity effect, the denser phase tends to move downward, and in the contrary, the lighter phase tends to move upward due to the buoyancy forces. The downward movement of the water with dissolved CO_2 appears in the shape of fingers in the models. Different snapshots are taken after 3 months and 6 months of simulation, in which the fingers and how the convection develops and the fingers reaching bottom part of the tank are visible.

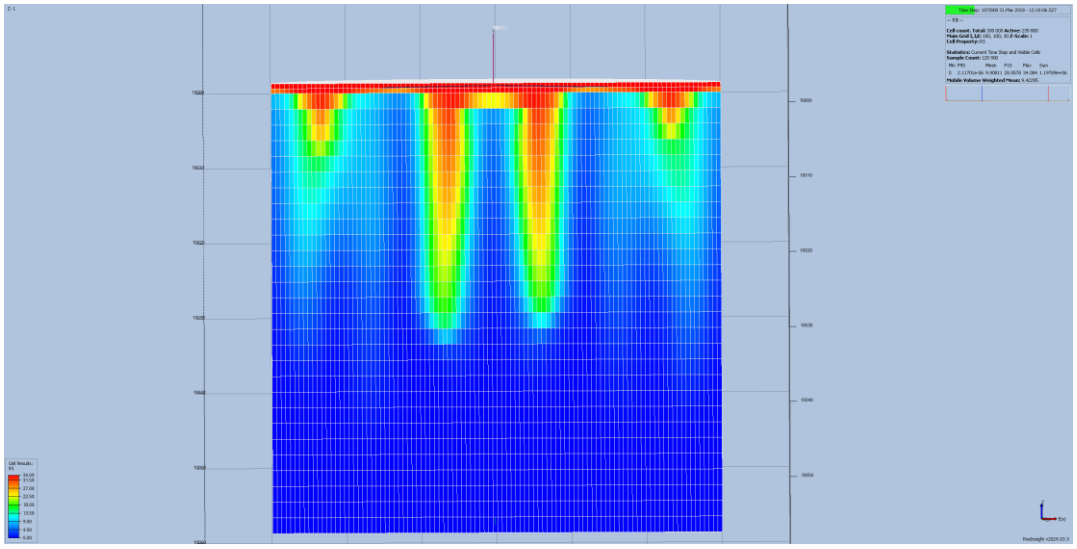

Figure 19- Development of convective mixing after three months of simulation

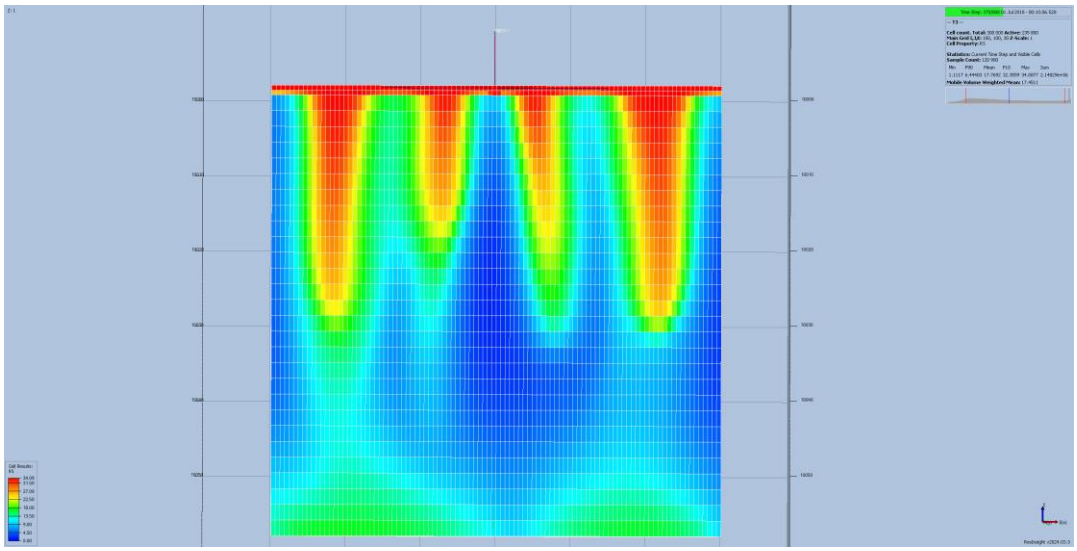

Figure 20- Development of convective mixing after six months of simulation

It can be seen from figure 22 that the tank is not fully saturated with the solution, and still there is a significant amount of pure water. This means that more CO_2 can dissolve until all the water reaches the maximum solubility. For better visualization, another snapshot after 6 months of simulation is taken with a threshold for Rs. This indicates that still a significant portion of water has no CO_2 dissolved and a huge portion has more capacity to dissolve more CO_2

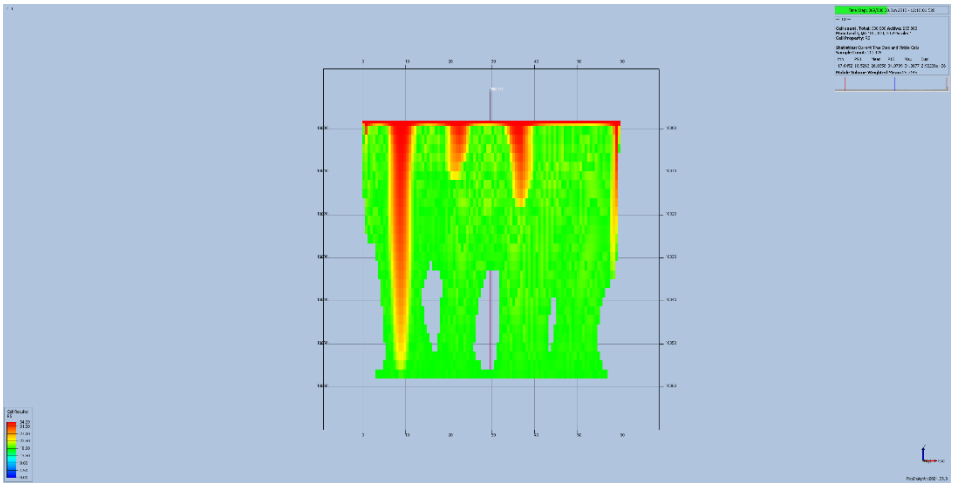

Figure 21- Dissolution distribution after 6 months of simulation with the threshold of Rs > 10

5.3 Impedance of Convection

After reaching the bottom of the tank, the flow of the solution tends to move laterally, occupying all the bottom part. This is what is happening at the macroscoping scale, while on the smaller scale, convection currents are happening in all parts of the porous media. The dissolution happens up to the point where there is no pure water. This is when the figure Rs over time platues. The following figures show full dissolution of gas into the water.

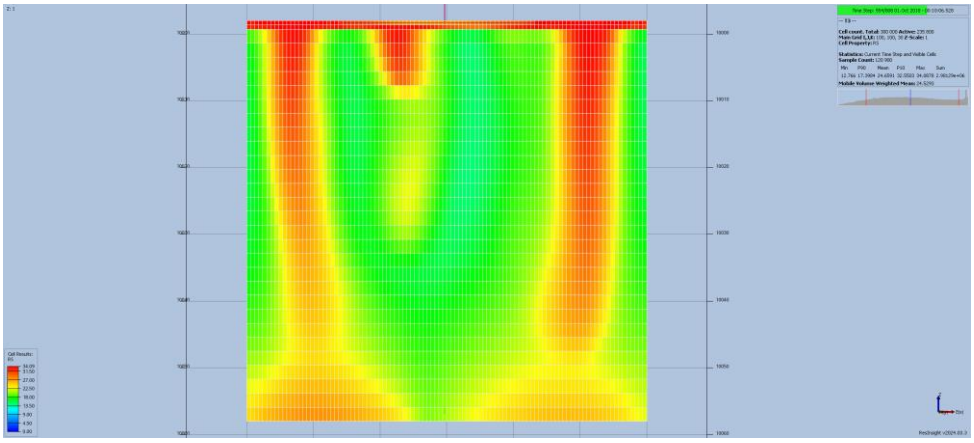

Figure 22- Convection developed; dissolution distribution after 9 months of simulation

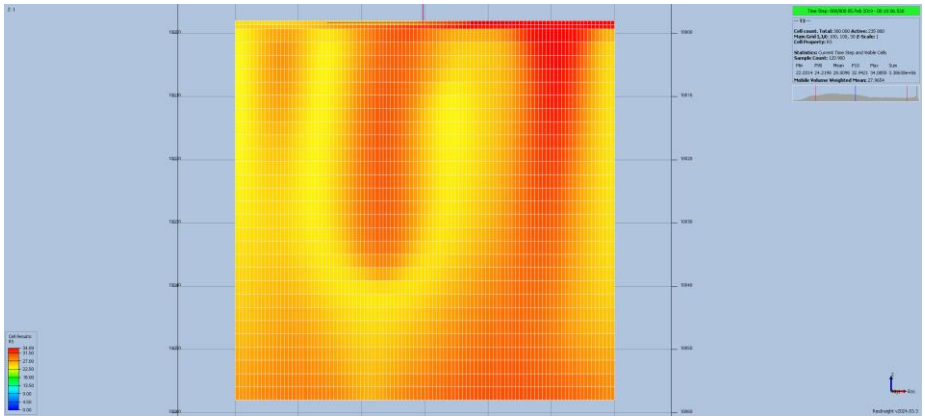

Figure 23- Convection impedance; dissolution distribution after 14 months of simulation

6. Conclusion

The Primary objective of this research was to understand the behavior of the gas when injected in water and its contribution to dissolution trapping in CO_2 storage applications. Achieving these goals require relatively high resolution data availability, a descent initial model with time-to-time refinement and data analysis.

6.1 Key findings

Diffusion Contribution: It is clear that diffusion is not making a significant contribution to the dissolution. However, it is the key factor that impacts the strength of the convection.

Capillary Pressure: Capillary forces prevent the gas from dissolving into the water at the very early time of injection. Nevertheless, this does not mean that they are acting against the dissolution. They let the gas accumulate at the top which causes higher concentration gradients and thus, stronger diffusion into the water.

Relative Permeability: Although there is minimal flow in the simulation in the gas filling step and there is not a multiphase flow after that, linear relative permeability may not accurately model the lateral movement of the gas at early time of injection due to presence of a small portion of the water there, if used. Therefore, a curved model, Brooks-Corey for example, may be a more precise approach to be used.

Initialization: Due to the nature of the simulation, which represents a model in laboratory scale, the model cannot be initialized with regular parameters such as initial pressure,

datum depth and contacts. Instead, enumeration method can be used to initialize the model by explicitly entering pressures, solution gas water ratio and saturations.

Discretization: To fully explore different regimes in dissolution trapping, the accuracy and resolution of the simulation is highly dependent on the grid cell size and number. Small grids can give a more precise answer of the system. However, it should be noted that the smaller and the higher the number of grid cells, the higher the simulation time is. So, optimization on grid size is significantly important.

6.2 Limitations

Data Availability: Due to the failure of the experiments a few weeks after it began, the model could not be refined to match the real case, thus predicting the dissolution amount and rate based on the system behavior in the laboratory.

Simulator: Eclipse 100 might not be appropriate software to perform such simulation as it is wildly used in field-scale simulations rather than lab-scale. During the simulation process, there were convergence error multiple times, and dealing with such error require more time and focus.

Computational Constraints: As the simulation runs were highly time-consuming, it was not possible to focus in all the aspects of the process which affect the precision of the outputs. More sensitivity analysis may lead to more accurate results.

6.3 Recommendation for Future Work

Use of Other Simulators or open-source codes: Using alternative software which can better perform small scale modelling may help enhancing the outputs quality. In addition, open-source codes and python libraries developed previously which have open access can be used to improve the simulations.

Discretization Optimization: Optimizing the grid sizing and number with AI or other tools can highly impact the performance of the work.

6.4 Final Thoughts

This research has been done to explore the nature of the CO_2 dissolution in saline aquifers in a real case application. While significant research has been performed and exist in the

literature, this research demonstrated that there are still a lot of room to discuss the potential challenges of this process with possible solutions to fully understand how dissolution trapping occurs, and which parameters significantly impact on it.

References

[1] N. O. a. A. A. (NOAA). [Online]. Available: https://gml.noaa.gov/ccgg/trends/.

[2] F. M. J. Orr, "Storage of Carbon Dioxide in Geological Formations," *Journal of Petroleum Technology,* vol. 56, no. (3), pp. 90-97, September 2004.

[3] S. Bachu, "Screening and ranking of sedimentary basins for sequestration of CO2 in geological media in response to climate change," *Environ Geol,* vol. 44, pp. 277-289, 2003.

[4] IPCC, 2005: IPCC Special Report on Carbon Dioxide Capture and Storage. Prepared by Working Group III of the Intergovernmental Panel on Climate Change [Metz, B., O. Davidson, H. C. de Coninck, M. Loos, and L. A. Meyer (eds.)]. Cambridge University Press, Cambridge, United Kingdom and New York, NY, USA, 442 pp.

[5] Bert Metz et al. "Carbon dioxide capture and storage". Cambridge University,New York, 2005. isbn: 9780521866439.

[6] Cal Cooper. “A Technical Basis for Carbon Dioxide Storage”. In: Energy Procedia 1 (Feb. 2009), pp. 1727–1733. doi: 10.1016/j.egypro.2009.01.226.

[7] G.P.D. De Silva, P.G. Ranjith, and M.S.A. Perera. “Geochemical aspects ofCO2 sequestration in deep saline aquifers: A review”. In: Fuel 155 (2015),pp. 128–143. issn: 0016-2361. doi: https://doi.org/10.1016/j.fuel.2015.03.045. url: https://www.sciencedirect.com/science/article/pii/S0016236115003415.

[8] Zhihua Zhang and Donald Huisingh. “Carbon dioxide storage schemes: Technology,assessment and deployment”. In: Journal of Cleaner Production 142(2017), pp. 1055–1064. issn: 0959-6526. doi: https://doi.org/10.1016/j.jclepro.2016.06.199. url:https://www.sciencedirect.com/science/article/pii/S0959652616308861.

[9] C.D. Hawkes, P.J. McLellan, and S. Bachu. “Geomechanical Factors Affecting Geological Storage of CO2 in Depleted Oil and Gas Reservoirs”. In: Journal of Canadian Petroleum Technology 44.10 (Oct. 2005). issn: 0021-9487. doi: 10.2118/05-10-05. eprint: https://onepetro.org/JCPT/articlepdf/doi/10.2118/05- 10- 05/2175048/petsoc- 05- 10- 05.pdf. url: https://doi.org/10.2118/05-10-05.

[10] Fatima Al Hameli, Hadi Belhaj, and Mohammed Al Dhuhoori. “CO2 Sequestration Overview in Geological Formations: Trapping Mechanisms Matrix Assessment”. In: Energies 15.20 (2022). issn: 1996-1073. doi: 10.3390/en15207805. url: https://www.mdpi.com/1996-1073/15/20/7805.

[11] N. Ahmed Khan. Project Report – “CO2 Storage in a Generic Depleted GasReservoir Model”. TPG4560 Petroleum Engineering, Specialization Project. 2021.

[12] International Energy Agency. CO2 Storage Resources and their Development. Accessed: 2024-06-27. International Energy Agency. 2022. url: https://www.iea.org/reports/co2- storageresources-and-their-development.

[13] Bachu, Stefan, W. D. Gunter, and E. H. Perkins. "Aquifer disposal of CO2: hydrodynamic and mineral trapping." *Energy Conversion and management* 35.4 (1994): 269-279.

[14] Akbarabadi, Morteza, and Mohammad Piri. "Relative permeability hysteresis and capillary trapping characteristics of supercritical CO2/brine systems: An experimental study at reservoir conditions." *Advances in Water Resources* 52 (2013): 190-206.

[15] Juanes, Ruben, et al. "Impact of relative permeability hysteresis on geological CO2 storage." *Water resources research* 42.12 (2006).

[16] Dongxiao Zhang and Juan Song. “Mechanisms for Geological Carbon Sequestration”. In: Procedia IUTAM 10 (2014). Mechanics for the World: Proceedings of the 23rd International Congress of Theoretical and Applied Mechanics, ICTAM2012, pp. 319–327. issn: 2210-9838. doi: https://doi.org/10. 1016/j.piutam.2014.01.027. url: https://www.sciencedirect.com/science/article/pii/S2210983814000285.

[17] Erik Lindeberg and Dag Wessel-Berg. “Vertical convection in an aquifer column under a gas cap of CO2”. In: Energy Conversion and Management 38 (1997). Proceedings of the Third International Conference on Carbon Dioxide Removal, S229–S234. issn: 0196-8904. doi: https://doi.org/10.1016/S0196-8904(96)00274-9. url: https://www.sciencedirect.com/science/article/pii/S0196890496002749.

[18] Temitope Ajayi, Jorge Gomes, and Achinta Bera. “A review of CO2 storage in geological formations emphasizing modeling, monitoring and capacity estimation approaches”. In: Petroleum Science 16 (July 2019), pp. 1–36. doi: 10.1007/s12182-019-0340-8.

[19] P. M. Sigmund. Prediction of Molecular Diffusion at Reservoir Conditions. Part 1 – Measurement and Prediction of Binary Dense Gas Diffusion Coefficients. Petroleum Society of Canada, 1976.

[20] Lowney, J. R., and R. D. Larrabee. "The use of Fick's law in modeling diffusion processes." *IEEE Transactions on Electron Devices* 27.9 (1980): 1795-1798.

[21] Apostolos Kantzas, Jonathan Bryan, and Saeed Taheri. Fundamentals of Fluid Flow in Porous Media. https : / / www . coursehero . com / file / 52594718/262639210-Fundamentals-of-Fluid-Flow-in-Porous-Mediav1-2-2014-11-11-Pdf0pdf/. Accessed on: <date>. 2014.

[22] Riti Gupta, 16 Feb. 2020. Four Things That Affect Rate of Diffusion. (Accessed: 06 November 2023). url: https://sciencing.com/four-thingsaffect-rate-diffusion-8348637.html.

[23] Hassan Hassanzadeh et al. “Predicting PVT data for CO2–brine mixtures for black-oil simulation of CO2 geological storage”. In: International Journal of Greenhouse Gas Control 2.1 (2008), pp. 65 77. issn: 1750-5836. doi: https : / / doi . org / 10 . 1016 / S1750 - 5836(07) 00010 - 2. url: https : //www.sciencedirect.com/science/article/pii/S1750583607000102.

[24] Jiajun Cen. “Simulations of Density Driven Convection in Porous Media”. Dissertation. Doctor of Philosophy in Chemical Engineering. Imperial College London, 2019.

[25] Hassan Hassanzadeh, Mehran Pooladi-Darvish, and David Keith. “Modelling of Convective Mixing in CO2 Storage”. In: Journal of Canadian Petroleum Technology 44 (Jan. 2004). doi: 10.2118/2004-151.

[26] Lindeberg, E., & Wessel-Berg, D. (2011). Upscaling studies of diffusion-induced convection in homogeneous and heterogeneous aquifers. Sintef Petroleum Research, S.P. Andersens vei 15b, N-7465 Trondheim, Norway. https://doi.org/10.1016/j.egypro.2011.02.331

[27] Sclumberger (2024), Eclipse 100 Reference Manual and Technical Manual

[28] https://resinsight.org/

[29] H. M. Polat, F. M. Coelho, T. J. H. Vlugt, L. F. Mercier Franco, I. N. Tsimpanogiannis, and O. A. Moultos, "Diffusivity of CO2 in H2O: A Review of Experimental Studies and Molecular Simulations in the Bulk and in Confinement," *J. Chem. Eng. Data*, vol. 69, no. 10, pp. 3296–3329, 2024, doi: 10.1021/acs.jced.3c00778.

[30] F. Doster, J. M. Nordbotten, and M. A. Celia, "Impact of capillary hysteresis and trapping on vertically integrated models for CO2 storage," *Dep. of Civil and Environmental Engineering, Princeton University*, Princeton, NJ, USA, and *Dep. of Mathematics, University of Bergen*, Bergen, Norway.